Preprints of the 19th World Congress
The International Federation of Automatic Control
Cape Town, South Africa. August 24-29, 2014

A comparison between Internal Model Control, optimal PIDF and robust controllers for unstable flow in risers

E. Jahanshahi, V. De Oliveira, C. Grimholt, S. Skogestad [1]

Department of Chemical Engineering, Norwegian Univ. of Science and technology, Trondheim, NO-7491 (e-mail: skoge@ntnu.no).

Abstract: Anti-slug control of multiphase risers involves stabilizing an open-loop unstable operating point. PID control is the preferred choice in the industry, but appropriate tuning is required for robustness. In this paper, we define PIDF as a PID with a low-pass filter on its derivative action where the low-pass filter is crucial for the dynamics. We compared a new PIDF tuning based on Internal Model Control (IMC), together with two other tunings from the literature, with an optimal PIDF controller. The optimal PIDF tuning was found by minimizing a performance cost function while satisfying robustness requirements (input usage and complementary sensitivity peak). Next, we considered two types of robust $\mathcal{H}_\infty$ controller (mixed-sensitivity and loop-shaping). We compared the controllers based on their pareto-optimality, and we tested the controllers experimentally. We found that the new IMC-PIDF controllers is the closest to the optimal PIDF controller, but the robustness can be further improved by $\mathcal{H}_\infty$ loop-shaping.

Keywords: Anti-slug control, unstable systems, robust control, Internal Model Control

1. INTRODUCTION

The severe-slugging flow regime which is common at offshore oilfields is characterized by large oscillatory variations in pressure and flow rates. This multi-phase flow regime in pipelines and risers is undesirable and an effective solution is needed to suppress it (Godhavn et al., 2005). One way to prevent this behaviour is to reduce the opening of the top-side choke valve. However, this conventional solution reduces the production rate from the oil wells. The recommended solution to maintain a non-oscillatory flow regime together with the maximum possible production rate is active control of the topside choke valve (Havre et al., 2000). Measurements such as pressure, flow rate or fluid density are used as the controlled variables and the topside choke valve is the main manipulated variable.

Existing anti-slug control systems are not robust and tend to become unstable after some time, because of inflow disturbances or plant changes. The main objective of our research is to find a robust solution for anti-slug control systems. The nonlinearity of the system is problematic for stabilization as the gain changes drastically between different operating conditions. In addition, another difficulty for stabilization is the effective time delay .

One solution is to use nonlinear model-based controllers to counteract the nonlinearity (e.g. Di Meglio et al., 2010). However, we have found that these solutions are not robust against time delays or plant/model mismatch (Jahanshahi and Skogestad, 2013b).

An alternative approach is to use PID controllers to stabilize the unstable flow. The PI and PID controllers are still the most widely used controllers in the industry and even from the academic point of view they are unbeatable in combined robustness and performance.

The purpose of this paper is to verify different tuning rules when applied to anti-slugging control and to give recommendations about the most appropriate rules to use. For this, we compare PID controllers with optimal controllers in simulations and experiments.

Jahanshahi and Skogestad (2013a) showed that a linear model with two unstable poles and one stable zero is sufficient for designing an anti-slug controller. They identified such a model from a closed-loop step test and proposed a PIDF tuning based on Internal Model Control (IMC) for this system. This tuning rules were slightly modified by including the derivative action filter.

We here define a four-parameter PIDF controller as a PID controller with filtered derivative action (Åström and Hägglund, 2006).

$$K_{\text{PIDF}}(s) = K_p + \frac{K_i}{s} + \frac{K_d s}{T_f s + 1} \tag{1}$$

where K_p is the proportional gain, K_i is the integral action gain, K_d is the derivative action gain and T_f is the filter time constant. We differentiate this from a standard PID controller, because the low-pass filter is a crucial part of the controller for our application. That is, the filter time constant cannot be reduced without sacrificing performance.

One of the optimal controllers used for the comparison, is a PIDF where optimal tuning are found by minimizing

[1] Corresponding author

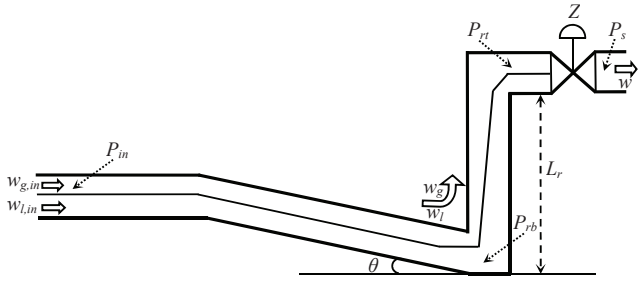

Fig. 1. Schematic presentation of system

a performance cost function while specifying robustness requirement (input usage and complementary sensitivity peak). Then, we consider use of two $\mathcal{H}_\infty$ robust controllers. $\mathcal{H}_\infty$ mixed-sensitivity design minimizes $\overline{\sigma}(S)$ for performance, $\overline{\sigma}(T)$ for robustness and low sensitivity to noise, and $\overline{\sigma}(KS)$ to penalize large inputs. In $\mathcal{H}_\infty$ loop-shaping design, we specify an initial plant loop shape, then the loop-shaping procedure increases robustness by maximizing the stability margin (Skogestad and Postlethwaite, 2005). The PIDF controller found by (Jahanshahi and Skogestad, 2013a) is used to make the initially shaped plant for the loop-shaping design.

For sake of completeness, we have also included in our study the simple PID tuning rules for unstable processes proposed by Rao and Chidambaram (2006) and Lee et al. (2006).

This paper is organized as follows. Section 2 describes the pipeline-riser system. The new PIDF tuning is presented in Section 3, and the optimal PIDF tuning is introduced in Section 4. Mixed-sensitivity and loop-shaping designs are presented in Section 5 and Section 6, respectively. The results are presented in Section 7. Finally, we summarize the main conclusions and remarks in Section 8.

2. SYSTEMS DESCRIPTION

Fig. 1 shows a schematic presentation of the system. The inflow rates of gas and liquid to the system, $w_{g,in}$ and $w_{l,in}$, are assumed to be independent disturbances and the top-side choke valve opening ($0 < Z < 100\%$) is the manipulated variable. A fourth-order dynamic model for this system was presented by Jahanshahi and Skogestad (2011). The state variables of this model are as:

- m_{gp}: mass of gas in pipeline [kg]
- m_{lp}: mass of liquid in pipeline [kg]
- m_{gr}: mass of gas in riser [kg]
- m_{lr}: mass of liquid in riser [kg]

The four state equations of the model are

$$\dot{m}_{gp} = w_{g,in} - w_g \tag{2}$$
$$\dot{m}_{lp} = w_{l,in} - w_l \tag{3}$$
$$\dot{m}_{gr} = w_g - \alpha w \tag{4}$$
$$\dot{m}_{lr} = w_l - (1-\alpha) w \tag{5}$$

The flow rates of gas and liquid from the pipeline to the riser, w_g and w_l, are determined by pressure drop across the riser-base where they are described by virtual valve equations. The outlet mixture flow rate, w, is determined by the opening percentage of the top-side choke valve, Z. The different flow rates and the gas mass fraction, α, in the equations (2)-(5) are given by additional model equations given by Jahanshahi and Skogestad (2011).

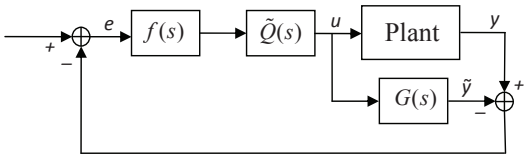

Fig. 2. Block diagram of Internal Model Control system

However, Jahanshahi and Skogestad (2013a) showed that a second-order model with two unstable poles and one stable zero is enough for the control design purposes, and such a model can be identified by a closed-loop step test.

3. PIDF TUNING BASED ON IMC DESIGN

3.1 IMC design for unstable systems

The Internal Model Control (IMC) design procedure is summarized by Morari and Zafiriou (1989). The block diagram of the IMC structure is shown in Fig. 2. Here, $G(s)$ is the nominal model which in general has some mismatch with the real plant $G_p(s)$. $\tilde{Q}(s)$ is the inverse of the minimum phase part of $G(s)$ and $f(s)$ is a low-pass filter for robustness of the closed-loop system.

The IMC configuration in Fig. 2 cannot be used directly for unstable systems; instead we use the conventional feedback structure with the stabilizing controller

$$C(s) = \frac{\tilde{Q}(s) f(s)}{1 - G(s)\tilde{Q}(s) f(s)}. \tag{6}$$

For internal stability, $\tilde{Q}f$ and $(1 - G\tilde{Q}f)$ have to be stable. We use the identified model with two unstable poles and one stable zero (Jahanshahi and Skogestad, 2013a) as the plant model:

$$G(s) = \frac{\hat{b}_1 s + \hat{b}_0}{s^2 - \hat{a}_1 s + \hat{a}_0} = \frac{k'(s+\varphi)}{(s-\pi_1)(s-\pi_2)} \tag{7}$$

and we get

$$\tilde{Q}(s) = \frac{(1/k')(s-\pi_1)(s-\pi_2)}{s+\varphi} \tag{8}$$

We design the filter $f(s)$ as explained by Morari and Zafiriou (1989), which gives the following third order filter

$$f(s) = \frac{\alpha_2 s^2 + \alpha_1 s + \alpha_0}{(\lambda s + 1)^3}, \tag{9}$$

where λ is an adjustable closed-loop time-constant. We choose $\alpha_0 = 1$ to get integral action and the coefficients α_1 and α_2 are calculated by solving the following system of linear equations:

$$\begin{pmatrix} {\pi_1}^2 & \pi_1 & 1 \\ {\pi_2}^2 & \pi_2 & 1 \end{pmatrix} \begin{pmatrix} \alpha_2 \\ \alpha_1 \\ \alpha_0 \end{pmatrix} = \begin{pmatrix} (\lambda\pi_1 + 1)^3 \\ (\lambda\pi_2 + 1)^3 \end{pmatrix} \tag{10}$$

Finally, from (6) the feedback version of the IMC controller becomes (Jahanshahi and Skogestad, 2013a)

$$C(s) = \frac{[\frac{1}{k'\lambda^3}](\alpha_2 s^2 + \alpha_1 s + 1)}{s(s+\varphi)}. \tag{11}$$

3.2 PIDF implementation of IMC controller

The IMC controller in (11) is a second order transfer function which can be written in form of a PID controller with a low-pass filter.

$$K_{\text{PIDF}}(s) = K_p + \frac{K_i}{s} + \frac{K_d s}{T_f s + 1} \tag{12}$$

where

$$T_f = 1/\varphi \tag{13}$$

$$K_i = \frac{T_f}{k' \lambda^3} \tag{14}$$

$$K_p = K_i \alpha_1 - K_i T_f \tag{15}$$

$$K_d = K_i \alpha_2 - K_p T_f \tag{16}$$

For the controller work in practice, we require that $K_p < 0$ and $K_d < 0$; and we must choose λ such that these two conditions are satisfied.

4. OPTIMAL PIDF CONTROL

For comparison purpose, we will define an optimal PIDF controller. However, optimality is generally difficult to define as we need to balance various factors such as output performance, robustness, input usage and noise sensitivity. We follow Grimholt and Skogestad (2012) and define the output performance as a weighted sum of the integrated square error (ISE) for disturbance at the plant input and output. However, a controller with good performance (low J) may not be robust. Thus, Grimholt and Skogestad (2012) proposed to optimize J for a given robustness (M_s value). This gives a set of pareto-optimal controllers. However, we found that for our application it was necessary to add a third dimension to constraint the input usage (M_{ks}). This results in a pareto optimal surface.

4.1 Evaluation of performance, robustness and input usage

Performance: Output performance is related to the difference between the measurement $y(t)$ and the setpoint y_s, and can be quantified in several different ways. In this paper we chose to quantify the performance in terms of a single scalar, namely the integrated squared error:

$$\text{ISE} = \int_0^\infty (y(t) - y_s(t))^2 \, dt \tag{17}$$

To balance the servo/regulatory trade-off we choose a weighted average of ISE for a step input load disturbance d_i and ISE for a step output load disturbance d_o:

$$J(K) = 0.5 \left[\frac{\text{ISE}_{do}(K)}{\text{ISE}^\circ_{do}} + \frac{\text{ISE}_{di}(K)}{\text{ISE}^\circ_{di}} \right] \tag{18}$$

where K is a PIDF-controller. The weighting factors ISE°_{di} and ISE°_{do} are for reference PIDF-controllers, which for the given process is ISE-optimal for a step load change on input and output, respectively. More details about this formulation can be found in Grimholt and Skogestad (2012).

Robustness: Robustness can be quantified in several ways. Most commonly used is the sensitivity peak (M_s), complementarity sensitivity peak (M_t), gain margin (GM), phase margin (PM), and allowable time delay error ($\frac{\Delta\theta}{\theta}$). In this paper we have chosen to quantify robustness as

$$M = \max(M_s, M_t) \tag{19}$$

where $M_s = \|S\|_\infty = \max_\omega |S|$ and $M_t = \|T\|_\infty = \max_\omega |T|$ for all frequencies and

$$S = \frac{1}{1 + GK}, \qquad T = \frac{GK}{1 + GK} \tag{20}$$

$\| \cdot \|_\infty$ is the $\mathcal{H}_\infty$-norm, which gives the peak value in the frequency domain. A small M tells that large relative perturbations in the process transfer functions are permitted (Åström and Hägglund, 2006). Since our system is unstable, we will normally have $M = M_t$. For stable processes, however, we would generally have $M = M_s$.

Input usage: A major concern in our application is to limit the input usage. This can be achieved by limiting the magnitude peak $M_{ks} = \|KS\|_\infty = \max_\omega |KS|$, where

$$KS = \frac{K}{1 + GK} \tag{21}$$

4.2 Optimization problem:

The pareto optimal PIDF controller (K) was found by solving the following optimization problem

$$\min_K \quad J(K) = 0.5 \left[\frac{\text{ISE}_{do}(K)}{\text{ISE}^\circ_{do}} + \frac{\text{ISE}_{di}(K)}{\text{ISE}^\circ_{di}} \right]$$
$$\text{s.t.} \quad M = m; \quad M_{ks} = m_{ks} \tag{22}$$

for various combinations of m (the desired M value) and m_{ks} (the specified bound in the magnitude of the input signal).

Computing the optimal controller: We propose solving the above optimization problem using gradient based nonlinear programming (NLP) techniques due to their fast convergence properties. However, the reliability of such methods depends on the quality of the gradients used by the NLP solvers. For this purpose, we use forward sensitivity calculation to obtain the exact gradients ($\nabla_K J$) of the objective function with respect to the parameters of the controller. The forward sensitivity method principle resides on first calculating $E = \frac{dx}{dt}$, where x are the closed-loop states of the system, and then relating this to J through chain-rule. Following the derivation by Biegler (2010), E can be obtained by solving the system

$$\frac{dE}{dt} = \frac{\partial f}{\partial x} E(t) + \frac{\partial f^T}{\partial K}, \quad B(0) = 0 \tag{23}$$

where $f \equiv \frac{dx}{dt} = A(K)x + B(K)u$ represents the state-space model of the closed-loop system. The gradient is then computed by

$$\nabla_K J = \frac{\partial J}{\partial x} E(t_f) + \frac{\partial J}{\partial K} \tag{24}$$

Note that the required partial derivatives may be computed using automatic differentiation or symbolic differentiation tools. The analytical calculation of the constraint gradients is more involved and should be further investigated. Here, the constraint gradients are approximated by central differences. It is worth to point out that, due to the nonconvexity of the optimization problem, we are bound to converge to a local minimum. One possibility to overcome this problem is to initialize the NLP solver

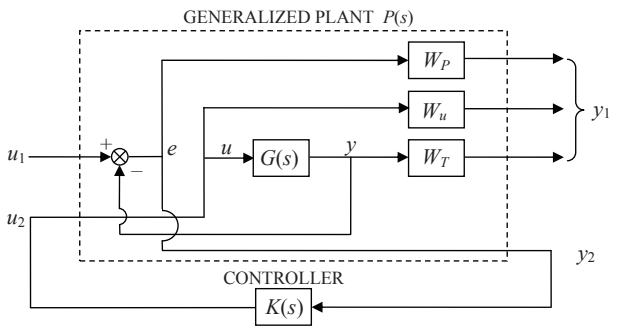

Fig. 3. Closed-loop system for mixed sensitivity control design

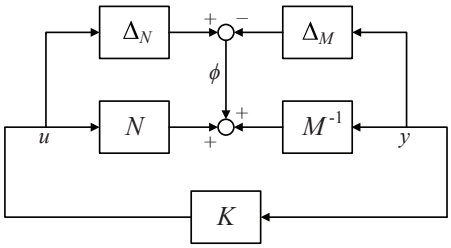

Fig. 4. $\mathcal{H}_\infty$ robust stabilization problem

with several different initial guesses and then choose the best overall solution. Alternatively, one may use a global optimization approach.

5. $\mathcal{H}_\infty$ MIXED-SENSITIVITY DESIGN

We consider an $\mathcal{H}_\infty$ problem where we want to bound $\overline{\sigma}(S)$ for performance, $\overline{\sigma}(T)$ for robustness and low sensitivity to noise, and $\overline{\sigma}(KS)$ to penalize large inputs. These requirements may be combined into a stacked $\mathcal{H}_\infty$ problem (Skogestad and Postlethwaite, 2005).

$$\min_K \|N(K)\|_\infty, \quad N \triangleq \begin{bmatrix} W_u KS \\ W_T T \\ W_P S \end{bmatrix} \tag{25}$$

where W_u, W_T and W_P determine the desired shapes of KS, T and S, respectively. Typically, W_P^{-1} is chosen to be small at low frequencies to achieve good disturbance attenuation (i.e., performance), and W_T^{-1} is chosen to be small outside the control bandwidth, which helps to ensure good stability margin (i.e., robustness). W_u is often chosen as a constant. The solution to this optimization problem gives a stabilizing controller K that satisfies (Doyle et al., 1989; Glover and Doyle, 1988):

$$\begin{aligned} \overline{\sigma}(KS(j\omega)) &\le \gamma \underline{\sigma}(W_u^{-1}(j\omega)) \\ \overline{\sigma}(T(j\omega)) &\le \gamma \underline{\sigma}(W_T^{-1}(j\omega)) \\ \overline{\sigma}(S(j\omega)) &\le \gamma \underline{\sigma}(W_P^{-1}(j\omega)) \end{aligned} \tag{26}$$

y_2 is the particular output for feedback control in the generalized plant in Fig. 3. The value of γ in equation (26) should be as small as possible for good controllability. However, it depends on the design specifications W_u, W_T and W_P.

6. $\mathcal{H}_\infty$ LOOP-SHAPING DESIGN

We consider the stabilization of the plant G which has a normalized left coprime factorization

$$G = M^{-1}N \tag{27}$$

A perturbed plant model G_p can then be written as

$$G_p = (M + \Delta_M)^{-1}(N + \Delta_N) \tag{28}$$

where Δ_M and Δ_N are stable unknown transfer functions which represent the uncertainty in the nominal plant model G. The objective of robust stabilization is to stabilize not only the nominal model G, but a family of perturbed plants defined by

$$G_p = \left\{(M + \Delta_M)^{-1}(N + \Delta_N) : \|[\Delta_N \;\; \Delta_M]\|_\infty < \epsilon\right\} \tag{29}$$

where $\epsilon > 0$ is then the stability margin (Skogestad and Postlethwaite, 2005). To maximize this stability margin is the problem of robust stabilization of normalized coprime factor plant description as introduced and solved by Glover and McFarlane (1989).

For the perturbed feedback system of Fig. 4, the stability property is robust if and only if the nominal feedback system is stable and

$$\gamma_K \triangleq \left\| \begin{bmatrix} K \\ I \end{bmatrix} (I - GK)^{-1} M^{-1} \right\|_\infty \le \frac{1}{\epsilon} \tag{30}$$

Notice that γ_K is the $\mathcal{H}_\infty$ norm from ϕ (see Fig. 4) to $\begin{bmatrix} u \\ y \end{bmatrix}$ and $(I - GK)^{-1}$ is the sensitivity function for this positive feedback arrangement. A small γ_K is corresponding to a large stability margin.

7. RESULTS

All the results (simulation and experimental) in this paper are based on the following model.

$$G(s) = \frac{-0.0098(s + 0.25)}{s^2 - 0.04s + 0.025} \tag{31}$$

This model was identified by Jahanshahi and Skogestad (2013a) from an experimental closed-loop step test around an operating point with the valve opening of $Z = 30\%$.

7.1 Pareto-Optimality Comparison

The optimization problem (22) was solved for a range of desired M_{ks} and M_t values using the linear model (31) (Here we assumed $M = M_t$ for all cases since we have an unstable system). This results of the optimizations form a Pareto front surface, which can be seen in Fig. 5. For simplicity, we did not include T_f as a degree of freedom in the optimization; instead, we fixed $T_f = 4$. This choice makes the filter counteract the effect of the zero of the plant, which is close to optimal this case. The NLP was solved using SNOPT Gill et al. (2005). Some points have been validated using brute force extensive search.

Figure 5 clearly depicts the trade-off between robustness, performance and input usage. The red line in Fig. 5 is the result from the IMC PIDF for different values of closed-loop time constant λ. By decreasing λ we get a faster controller with larger input usage M_{ks}, but M_t remains approximately constant. Note that the performance of the IMC PIDF is close to the pareto optimal surface for a large range of M_{ks}.

Figure 6 shows a cross-section of the PIDF Pareto surface with $M_{ks} = 50$, where the other controllers are also shown. All the controllers are tuned to give $M_{ks} = 50$.

Compared to Chidambaram-PIDF and Lee-PIDF, IMC-PIDF gives a better trade-off between robustness and performance. $\mathcal{H}_\infty$ loop-shaping controller gives a better combined performance and robustness. However, it is a higher order controller. Surprisingly, $\mathcal{H}_\infty$ mixed sensitivity gave a inferior performance compared to PIDF. Perhaps, a better performance could be achieved by a finer tuning of the weighting transfer functions W_P, W_T and W_u.

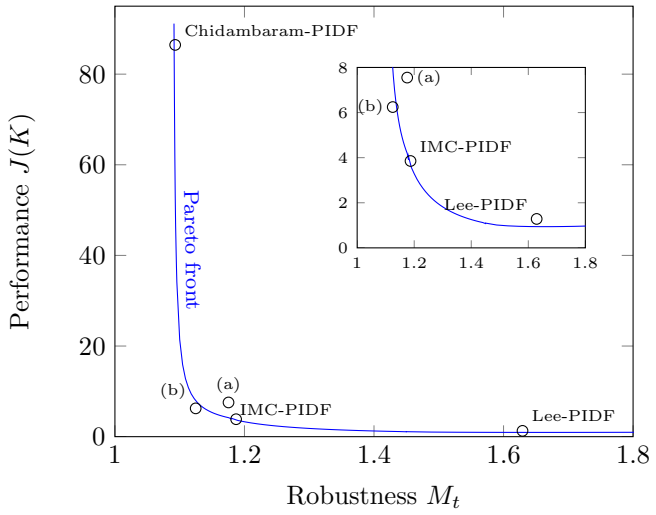

Fig. 6. Pareto front for $M_{ks} = 50$ for PIDF with $T_f = 4$. Point (a) represents the $\mathcal{H}_\infty$ mixed-sensitivity controller; point (b) represents the $\mathcal{H}_\infty$ loop-shaping controller.

7.2 Experimental setup

The experiments were performed on a laboratory setup for anti-slug control at the Chemical Engineering Department of NTNU. Fig. 7 shows a schematic presentation of the laboratory setup. The pipeline and the riser are made from flexible pipes with 2 cm inner diameter. The length of the pipeline is 4 m, and it is inclined with a 15° angle. The height of the riser is 3 m. A buffer tank is used to simulate the effect of a long pipe with the same volume, such that the total resulting length of pipe would be about 70 m.

The topside choke valve is used as the input for control. The separator pressure after the topside choke valve is nominally constant at atmospheric pressure. The feed into the pipeline is assumed to be at constant flow rates, 4 l/min of water and 4.5 l/min of air. With these boundary conditions, the critical valve opening where the system switches from stable (non-slug) to oscillatory (slug) flow is at $Z^* = 15\%$ for the top-side valve. The bifurcation diagrams are shown in Fig. 8.

The desired steady-state (dashed middle line) in slugging conditions ($Z > 15\%$) is unstable, but it can be stabilized by using control. The slope of the steady-state line (in the middle) is the static gain of the system, $k = \partial y/\partial u = \partial P_{in}/\partial Z$. As the valve opening increase this slope decreases, and the gain finally approaches to zero. This makes control of the system with large valve openings very difficult.

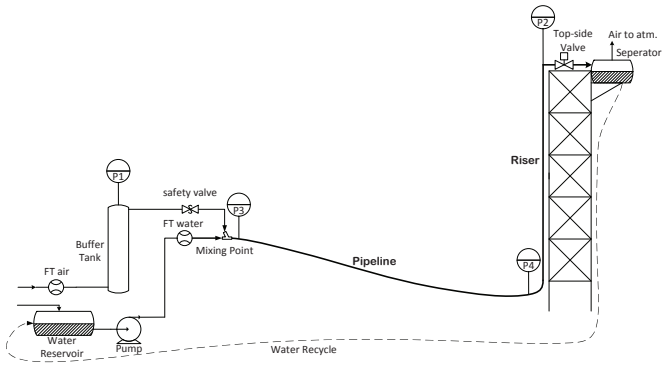

Fig. 7. Experimental setup

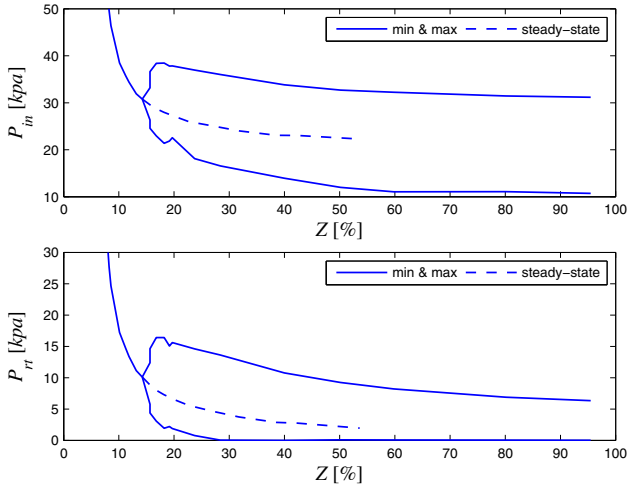

Fig. 8. Bifurcation diagrams for experimental setup

7.3 Experimental results

The controlled output in experiments is the inlet pressure of the pipeline (P_{in}) and we use the same set of descending pressure set-points in all experiments. As mentioned in above controlling the system with large valve openings (low pressure set-points) is difficult. We decrease the controller set-point to see if the controller can stabilize the system with lower set-point. The controllers are tuned (designed) for a valve opening of $Z = 30\%$, and controllers with good gain margin can stabilize the system with larger valve openings (lower set-points). To have an impartial comparison for robustness of the controllers, we tune the controllers with the same values of input usage ($M_{ks} = 50$). One interesting relationship for the KS peak of the PIDF controller in (12) can be written as follows.

$$M_{ks} = -(K_d/T_f + K_p) \tag{32}$$

Optimal PIDF: Fig. 9 and Fig. 10 show experimental result of two optimal PIDF controllers, optimal PIDF (1) and optimal PIDF (2). The controller tunings are given in Table. 1. The optimal PIDF (2) was optimized for a smaller values of M_t which resulted in a better gain margin and less oscillations is observed in Fig. 10 (better robustness). However, the optimal PIDF (2) yields higher values for ISE (Table. 1).

IMC PIDF : We used the identified model in (31) for an IMC design. We chose the filter time constant $\lambda = 6.666\ s$

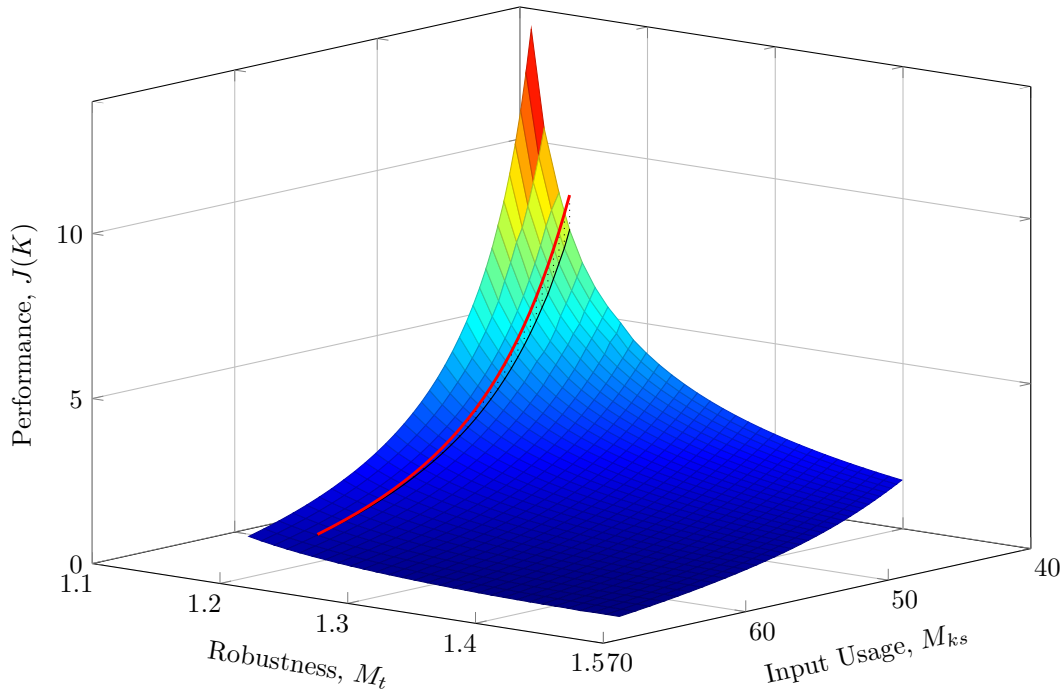

Fig. 5. Pareto optimal PIDF surface and IMC PIDF controller (red line).

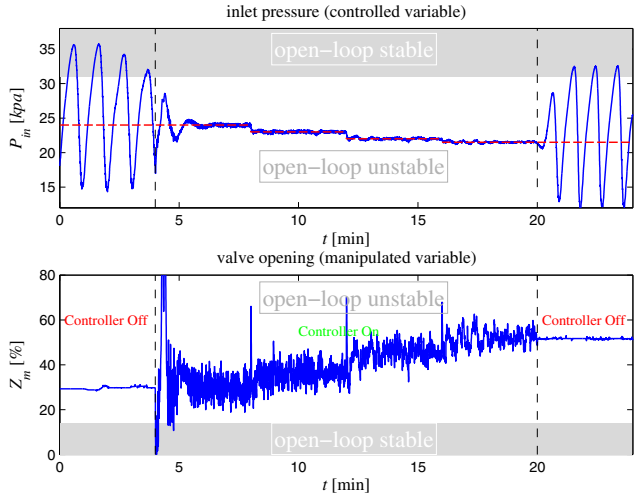

Fig. 9. Experimental result of optimal PIDF (1) with $K_p = -3.089$, $K_i = -1.62$, $K_d = -186.73$, $T_f = 4$

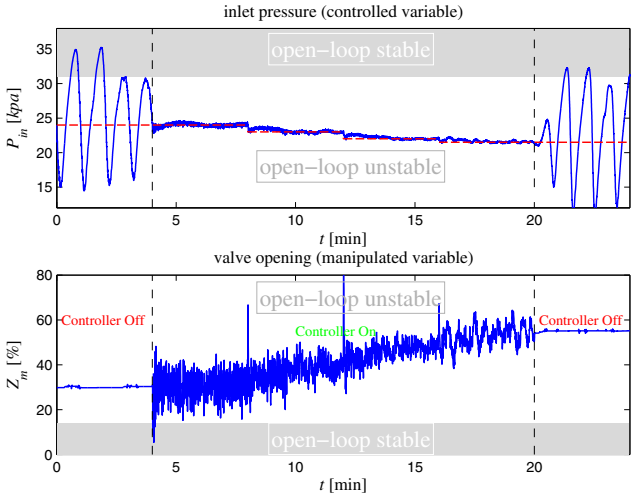

Fig. 10. Experimental result of optimal PIDF (2) with $K_p = 0.15$, $K_i = -0.198$, $K_d = -198.10$, $T_f = 4$

to get $M_{ks} = 50$. The resulting IMC controller becomes

$$C(s) = \frac{-50(s^2 + 0.0867s + 0.0069)}{s(s + 0.25)}. \qquad (33)$$

Note that the integral time for this controller is $\tau_I = {}^{K_p}/_{K_i} = 8.58$ s and the derivative time is $\tau_D = {}^{K_d}/_{K_p} = 12.89$ s. Since we have $\tau_I < 4\tau_D$, the zeros are complex and the controller cannot be implemented in cascade (series) form. The PIDF tuning resulted from this controller is given in Table. 1, and Fig. 11 shows performance of the IMC-PIDF controller in the experiment.

Chidambaram PIDF : The Chidambaram tuning (Rao and Chidambaram, 2006) is for systems with one zero, two unstable zeros and time delay. However, we do not have time delay our system, and we expect the tuning rules with $\theta = 0$ are still valid. The problem with this controller is that it does not have a low-pass filter on the derivative action; this results in a large KS peak and the controller becomes very aggressive. To solve this problem, we added the same low-pass filter as the one used in the IMC-PIDF controller. With this modification the Chidambaram tuning gives good results; the experimental result of this controller is shown in Fig. 12. We used $\tau_c = 20.17$ s to get $M_{ks} = 50$; the resulting tuning is given in Table. 1.

Lee PIDF : The Lee tuning (Lee et al., 2006) is based on analytic IMC-PIDF for first-order unstable systems with time delay. We had to approximate the model in (31) to a first-order model. We neglected the constant terms in the numerator and the denominator which are small values. This is same as what the model reduction

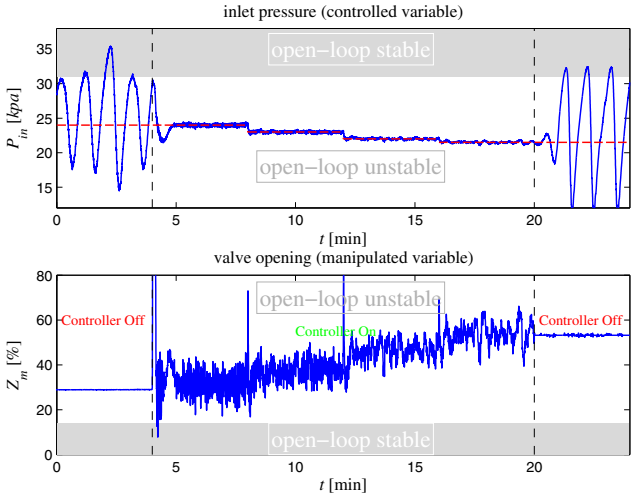

Fig. 11. Experimental result of IMC PIDF with $K_p = -11.84$, $K_i = -1.38$, $K_d = -152.65$, $T_f = 4$

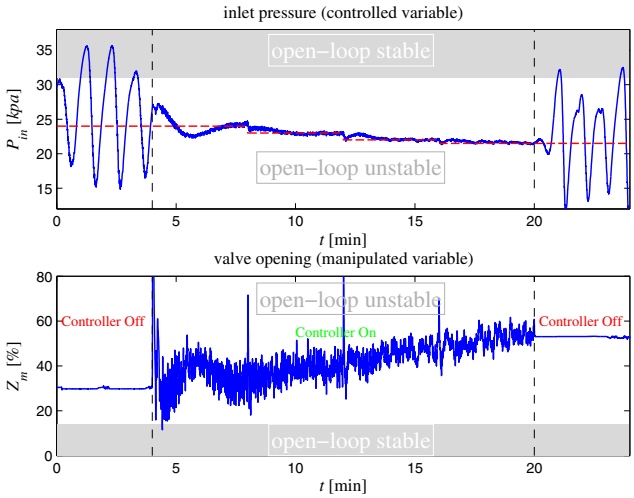

Fig. 12. Experimental result of Chidam. PIDF with $K_p = 1.69$, $K_i = -0.15$, $K_d = -206.91$, $T_f = 4$

toolbox of Matlab (*modred* routine with 'Truncate' option) does which preserves the high-frequency information. The reduced-order model is given in (34), and we used $\lambda = 5.35$ s to get $M_{ks} = 50$; the experimental result is shown in Fig. 13.

$$G_{red} = \frac{-0.245}{25s - 1} \tag{34}$$

$\mathcal{H}_\infty$ loop-shaping: We used the IMC-PIDF controller to obtain the initially shaped plant for the $\mathcal{H}_\infty$ loop-shaping design. The following fifth-order controller was resulted.

$$C(s) = \frac{-188.49(s^2 + 0.02s + 0.005)(s^2 + 0.087s + 0.0069)}{s(s + 0.25)(s + 3.76)(s^2 + 0.082s + 0.0067)} \tag{35}$$

The experimental result of the controller in (35) is shown in Fig. 14.

$\mathcal{H}_\infty$ mixed-sensitivity: We design the $\mathcal{H}_\infty$ mixed-sensitivity controller with the following design specifications:

$$W_P(s) = \frac{s/M_s + \omega_B}{s + \omega_B A}, \tag{36}$$

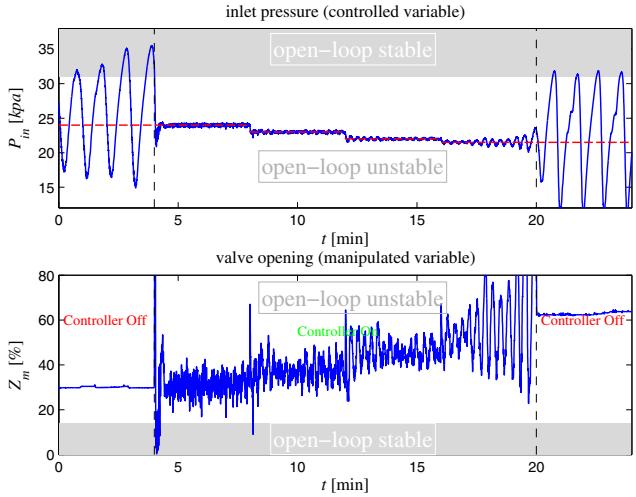

Fig. 13. Experimental result of Lee PIDF with $K_p = -41.05$, $K_i = -3.42$, $K_d = -0.082$, $T_f = 4$

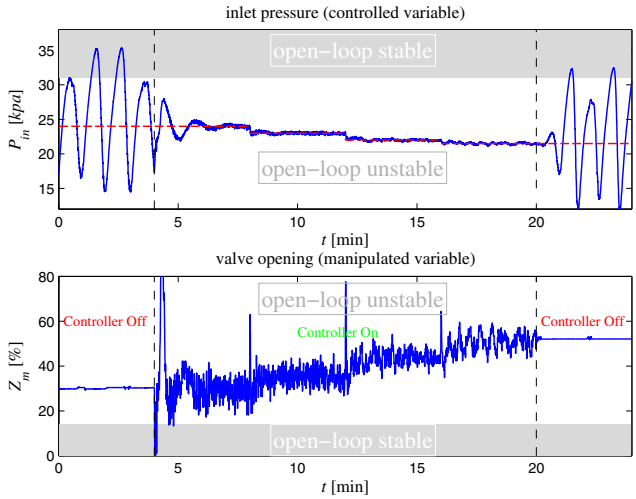

Fig. 14. Experimental result of loop-shaping $\mathcal{H}_\infty$

$$W_T(s) = \frac{s/(10\omega_B) + 1}{0.01s + 1}, \tag{37}$$

$$W_u = 0.0135, \tag{38}$$

where $M_s = 1$, $\omega_B = 0.14$ rad/s and $A = 0.01$. We chose these design specifications so that we achieve $M_{ks} = 50$ and good robustness properties. We get the following fourth-order stabilizing controller.

$$C(s) = \frac{-9.08\times10^6(s + 100)(s^2 + 0.0137s + 0.011)}{(s + 1.8 \times 10^5)(s + 112.5)(s + 0.231)(s + 0.0014)} \tag{39}$$

We achieved $\gamma = 1.21$ with this controller; the experimental performance is shown in Fig. 15.

8. CONCLUSION

In this paper we developed and compared feedback controllers for unstable multiphase flow in risers. The study included three sets of simple PIDF tuning rules, optimal PIDF and two $\mathcal{H}_\infty$ controllers. The comparison was based on Pareto optimality and experimental tests carried out in a prototype flow system. We showed that for this case the IMC-PIDF controllers are very close to the PIDF Pareto

Table 1. Comparison of different controllers in experiments

Controller	K_p	K_i	K_d	T_f	ISE	$\|S\|_\infty$	$\|T\|_\infty$	$\|KS\|_\infty$	GM	DM
Optimal PIDF (1)	-3.089	-1.62	-186.73	4	160.79	1.00	1.15	50	0.12	2.67
Optimal PIDF (2)	0.150	-0.198	-198.09	4	647.175	1.00	1.09	50	0.086	2.80
IMC PIDF	-11.84	-1.38	-152.65	4	171.45	1.00	1.19	50	0.11	2.49
Chidambaram PIDF	1.69	-0.15	-206.90	4	864.75	1.13	1.09	50	0.084	2.81
Lee PIDF	-41.05	-3.42	-0.08	4	726.88	1.20	1.62	50	0.17	1.70
$\mathcal{H}_\infty$ Loop Shaping	–	–	–	–	184.98	1.10	1.12	50	0.10	2.48
$\mathcal{H}_\infty$ Mixed Sensitivity	–	–	–	–	330.25	1.00	1.18	50	0.15	3.00

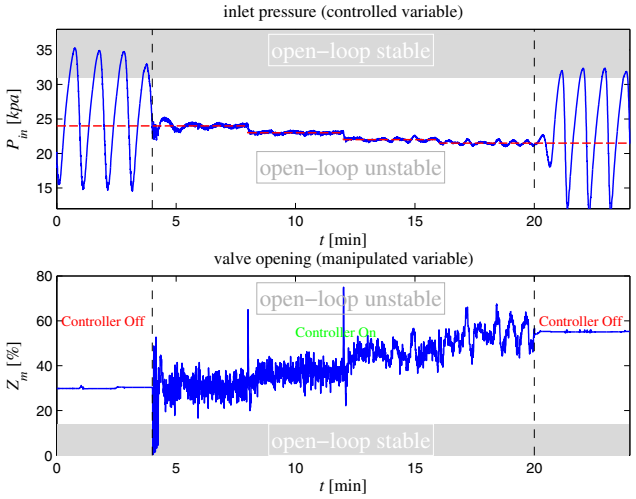

Fig. 15. Experimental result of mixed-sensitivity $\mathcal{H}_\infty$

optimal surface for a large range of the tuning parameter. Better results can be achieved by the $\mathcal{H}_\infty$ loop-shaping approach, where we employ the IMC-PIDF controller to obtain the initially shaped plant. However, this method results in higher order controllers which may not be desired by the practitioner. The $\mathcal{H}_\infty$ mixed-sensitivity design is more involved as it requires tuning of many weights simultaneously. However, we could not achieve better results than that of a PIDF controller for this case and further investigation is needed.

REFERENCES

Åström, K. and Hägglund, T. (2006). *Advanced PID Control*. ISA.

Biegler, L.T. (2010). *Nonlinear programming: Concepts, algorithms, and applications to chemical processes*. SIAM.

Di Meglio, F., Kaasa, G.O., Petit, N., and Alstad, V. (2010). Model-based control of slugging flow: an experimental case study. In *American Control Conference*, 2995–3002. Baltimore, USA.

Doyle, J., Glover, K., Khargonekar, P., and Francis, B. (1989). State-space solutions to standard $\mathcal{H}_2$ and $\mathcal{H}_\infty$ control problems. *IEEE Transactions on Automatic Control*, 34(8), 831–847.

Gill, P.E., Murray, W., and Sunders, M.A. (2005). SNOPT: An SQP Algorithm for Large-Scale Constrained Optimization. *SIAM Journal on Optimization*, 47(1), 99–131.

Glover, K. and Doyle, J.C. (1988). State-space formulae for all stabilizing controllers that satisfy an $\mathcal{H}_\infty$-norm bound and relations to relations to risk sensitivity. *Systems and Control Letters*, 11(3), 167–172.

Glover, K. and McFarlane, D. (1989). Robust stabilization of normalized coprime factor plant descriptions with h_∞-bounded uncertainty. *IEEE Transactions on Automatic Control*, 34(8), 821–830.

Godhavn, J.M., Fard, M.P., and Fuchs, P.H. (2005). New slug control strategies, tuning rules and experimental results. *Journal of Process Control*, 15, 547–557.

Grimholt, C. and Skogestad, S. (2012). Optimal PI-control and verification of the SIMC tuning rules. In *IFAC Conference on Advances in PID Control*. Brescia, Italy.

Havre, K., Stornes, K., and Stray, H. (2000). Taming slug flow in pipelines. *ABB Review*, 4, 55–63.

Jahanshahi, E. and Skogestad, S. (2011). Simplified dynamical models for control of severe slugging in multiphase risers. In *18th IFAC World Congress*, 1634–1639. Milan, Italy.

Jahanshahi, E. and Skogestad, S. (2013a). Closed-loop model identification and pid/pi tuning for robust anti-slug control. In *10th IFAC International Symposium on Dynamics and Control of Process Systems*. Mumbai, India.

Jahanshahi, E. and Skogestad, S. (2013b). Comparison between nonlinear modelbased controllers and gain-scheduling internal model control based on identified model. In *52nd IEEE Conference on Decision and Control*. Florence, Italy.

Lee, Y., Park, S., and Lee, M. (2006). Consider the generalized imc-pid method for pid controller tuning of time-delay processes. *Hybrocarbon Processing*, 6, 87–91.

Morari, M. and Zafiriou, E. (1989). *Robust Process Control*. Prentice Hall, Englewood Cliffs, New Jersey.

Rao, A.S. and Chidambaram, M. (2006). Control of unstable processes with two rhp poles, a zero and time delay. *Asia-Pacific Journal of Chemical Engineering*, 1(1-2), 63–69.

Skogestad, S. and Postlethwaite, I. (2005). *Multivariable Feedback Control: Analysis and Design*. Wiley & Sons, Chichester, West Sussex, UK.